Astronomy 121 Lab 3: Radio Interferometry at X Band

Vikram Iyer

April 8, 2014

Abstract

This lab experiment focused on understanding and using a multiplying interferometer composed of 2 1m dishes observing at X band separated by 10m along an approximately East-West baseline on the roof of Wurster Hall at UC Berkeley (37.8732, -122.2573) to observe the sun, moon, and various point sources. A least squares regression was used to approximate a function to fit the data and thereby determine an exact value for the baseline length using known catalog values for the declination of the source. Analysis of the strongest frequency components in the data from 3C144 (the Crab Nebula) showed the baseline distance to be 8.352m. A separate analysis with a very narrow bandwidth filter in what appears to be noise in the original spectrum yields a baseline value of 10.016m. A similar procedure was used to analyze the sun and moon data to determine their fringe frequency and thereby determine their radius by comparing the fringe frequency to an ideal Bessel function representing the intensity of these sources. The diameter of the sun was calculated to be 0.4312° and the diameter of the moon was determined to be $D = 0.34844^\circ$. This analysis used the assumed baseline distance of 10m rather than the value calculated from the analysis of the point source. Calculations of the cable delay from all analyses were inconclusive.

1 Introduction

Interferometry is a common tool in radio astronomy both for the purpose of correlating multiple signals to improve the signal to noise ratio (SNR) of weak astronomical signals, as well as to improve the resolution with which one can observe the sky. The purpose of this lab experiment was to learn and apply the basic principles of interferometry to measure the diameter of the sun and the moon, as well as the baseline length of the interferometer from the known declination of a point source. After recording and processing the raw data we applied least squares to obtain a function of best fit to the processed data in order to determine the quantities of interest such as source diameter and baseline.

2 Methods

2.1 Interferometer

We began this lab experiment by learning about the basics of interferometry as well as the details of the system we used for collecting data.

2.1.1 A Two Element Interferometer

A two-element interferometer consists of two telescopes separated by some baseline vector $\vec{b}$. Both telescopes receive radiation from the observed source and these signals are multiplied together to form the output. Because of the separation of the two telescopes, there is a delay between the time at which waves from the source reach the first telescope and the second one.

We can define the signals that each antenna detects as follows:

$$E_i(t) = e_1(t) + e_2(t)$$

$$E_j(t) = e_1(t - \tau_1) + e_2(t - \tau_2)$$

Correlating these received signals from the two antennas results in the average power received. The output of correlation should result in a set of values in the power spectrum which are significantly larger than the noise.

2.1.2 Wurster Hall Interferometer

The interferometer consists of two 1m diameter dishes along an approximately 10m East-West baseline located on the lower roof of Wurster Hall at UC Berkeley. Each antenna output is connected to a series of analog filters and amplifiers prior to sampling. After initial amplification and filtering at the source of the signal, the inputs are down converted from an original frequency of 10.7 GHz. This output is down converted again and filtered to a bandwidth of 30MHz. The outputs of the two dishes are then mixed and sampled. The data is collected by an HP digital voltmeter connected via GPIB to a Linux workstation. This computer is capable of both recording the output as well as controlling the motors to point the telescope. The full signal path is shown in 1.

This interferometer is mechanically limited to an altitude range of 15° to 87°. Additionally, tall buildings such as the Campanile and the other half of Wurster Hall further limit the interferometer's field of view. The interferometer can be pointed to a specified altitude and azimuth value within the range described, and can be updated less than every 30 seconds. The dishes' encoders do however accumulate error over time and must be reset to a home position every 2-3 hours.

2.2 Coordinate Transformations

In order to accurately point the interferometer at sources, we had to calculate the positions of sources and update them in real time. The point sources of interest all had known known right ascension (RA) and declination (DEC) values, however we had to convert these to an altitude and azimuth in order to point the telescope.

To perform the conversion we first converted the given coordinates from (RA, DEC) to (HA, DEC) by taking the dot product of the original coordinates as a vector with the following rotation matrices.

$$R_{(\alpha,\delta)\to(ha,\delta)} = R_{(\alpha,\delta)\to(ha,\delta),2} \cdot R_{(\alpha,\delta)\to(ha,\delta),1}$$

$$R_{(\alpha,\delta)\to(ha,\delta),1} = \begin{bmatrix} \cos(LST) & \sin(LST) & 0 \\ -\sin(LST) & \cos(LST) & 0 \\ 0 & 0 & 1 \end{bmatrix}$$

$$R_{(\alpha,\delta)\to(ha,\delta),2} = \begin{bmatrix} 1 & 0 & 0 \\ 0 & -1 & 0 \\ 0 & 0 & 1 \end{bmatrix}$$

After converting the values to terms of HA, which is dependent on a terrestrial position, we converted from (HA, DEC) to (ALT, AZ) based on our latitude ϕ using the following matrix.

$$R_{(ha,\delta)\to(az,alt)} = \begin{bmatrix} -\sin(\phi) & 0 & \cos(\phi) \\ 0 & -1 & 0 \\ \cos(\phi) & 0 & \sin(\phi) \end{bmatrix}$$

In order to accurately determine RA and DEC at the time of observation, we precessed the catalog values of RA and DEC for the epoch 2000. To perform this calculation we used the Python module PyEphem. In addition PyEphem contains useful options to calculate the altitude and azimuth of the sun and moon. This is particularly useful for the moon as it accounts for the effects of observing an object so close to the Earth. We also used the ephem.FixedBody object to actually perform the calculation of the altitude and azimuth for the point sources when collecting data. The details of the implementation can be found in observe.py.

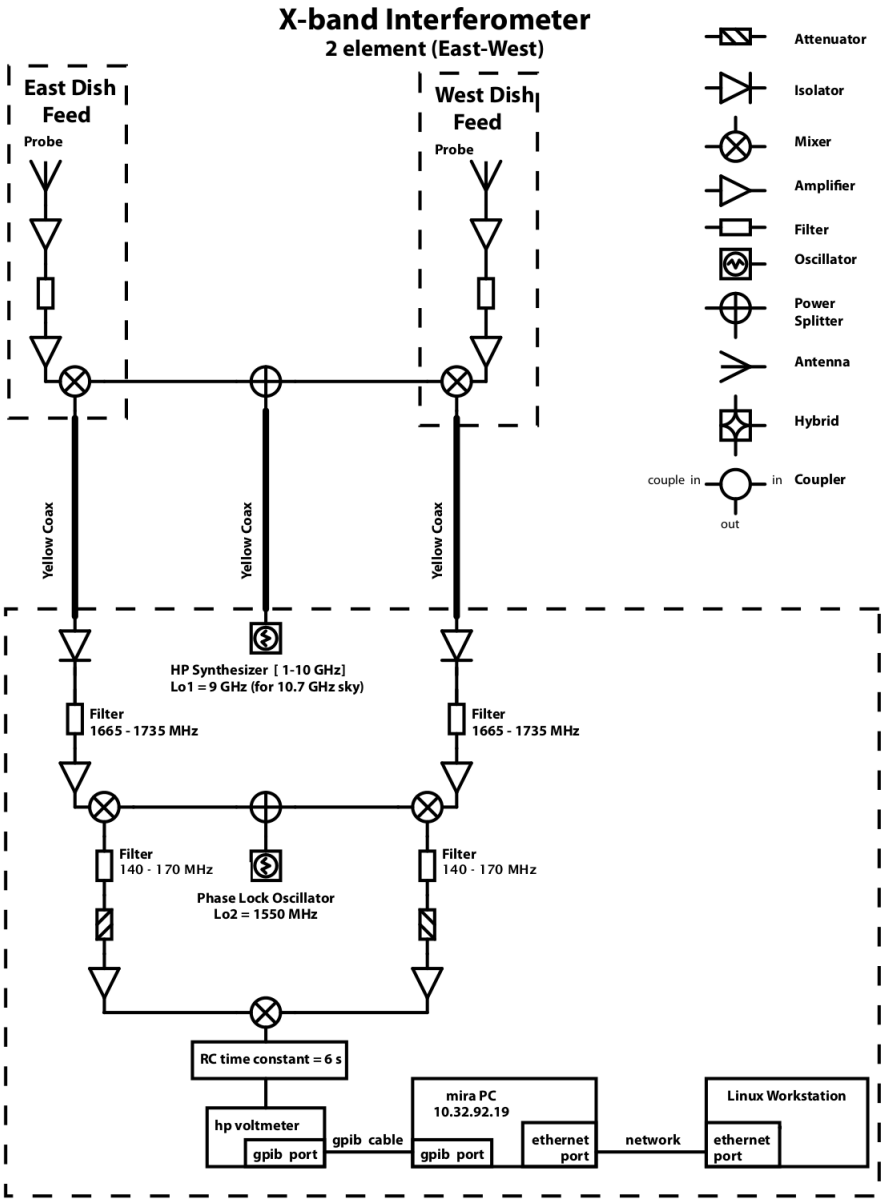

Figure 1: Block diagram of the interferometer on the roof of Wurster Hall.

2.3 Data Collection

As explained previously, the interferometer is connected to a Linux computer that is remotely accessible. In order to collect data, we had to ensure that the position of the interferometer was updated regularly to be directed at the source. Additionally we had to regularly reset the telescope to a reference position in order to prevent excessive accumulation of error from the encoders. We recalculated the position of the Sun and the Moon every 30 seconds as their position changed more quickly over time, and every 60 seconds for the point sources.

2.3.1 Data Collection Script

In order to automate our data collection, we wrote a Python script to calculate the position of the observed source at a given frequency as well as collect and save the data from the digital voltmeter (DVM). The script

itself is divided into two main functions that run in separate threads; the first of these functions controller calculates the position of the source every t seconds and re-points the telescope while the recordData function records data from the DVM and saves the output to a specified file. The source position updates were calculated based on updating the time of the ephem.Observer object used by PyEphem to compute the altitude and azimuth. As shown above, while our location on Earth was fixed, converting (RA,DEC) to (ALT, AZ) at a specific location requires the local sidereal time (LST) which we obtained using the ephem.now function.

Both the data record data and controller were run in separate threads so that we could record data continuously rather than having to pause and resume data collection to re-point the telescope every 30 seconds. In addition both threads were run as daemons to ensure consistency in the data (ie to account for cases in which the pointing may have failed, at which point recording data additional data would have been misleading). All functions used Python's logging utility to record detailed debug and warning messages for reference during data analysis. The full data collection script is available with detailed function documentation in observe.py.

2.3.2 Observed Sources

We observed a variety of sources including the Sun from horizon to horizon, as well as the Moon and point sources such as 3C144 (the Crab Nebula). We began by observing the Sun for a period of 1 hour, mainly to ensure that our data collection script was properly tracking and recording sources. After this we observed the Sun from horizon to horizon to gather data necessary for determining its diameter. We attempted to observe the moon multiple times, however most of these observations were within a few days of a new moon at which point only 15% of the moon was actually illuminated. We obtained an additional observation of the moon for 4 hours approximately a week after the new moon at which point 30% was illuminated. We attempted to observe multiple point sources including Orion, the Crab Nebula, and M17 as well.

2.4 Data Processing

Although the interferometer does correlate the signals received from the two telescopes, the radiation from most astronomical sources is negligible compared to other sources of electromagnetic radiation. while we were able to identify peaks corresponding to each source, the SNR was relatively low for all of the sources other than the sun. In order to process the data and calculate the values of interest, we attempted a variety of filtering techniques.

2.4.1 Point Souce Data

In order to isolate the frequencies corresponding to the point source, we attempted to filter the data in a variety of ways. These included a median filter to smooth the data, as well as band pass filters of varying bandwidth, windowing functions, and numbers of coefficients. We also attempted zeroing out entire ranges of values in the frequency domain and taking the inverse Fourier transform.

The general method we used for processing the point source data consisted of attempting to visually identify peaks corresponding to what were likely frequencies from the observed source. We also experimented with a few other ideas such as attempting to normalize the signal over a range of values, as the expected signal should have been roughly a constant amplitude. We also attempted analyzing subsections of the datasets for those in with some kind of unexpected behavior in the time domain.

2.4.2 Least Squares Fitting

After filtering the raw data, we applied least squares to fit a known model of the source to the measured values to determine the unknown parameters.

Ordinary least squares (OLS) corresponds to solving a simple optimization problem of the form

$$\min x||Ax - y||_2^2$$

This model is useful for estimating solutions to problems for which $Ax = y$ is not feasible. We there for project y onto Ax and attempt to minimize the squared Euclidean distance between them. The closed form solution to this problem is:

$$x* = (A^T A)^{-1} A^T y$$

In order to solve for the parameters corresponding to the equation for the interferometer output, we applied least squares. Although this model is nonlinear we assumed the function to be roughly linear considering $\sin(h_s)$ increases monotonically over time for a range of values.

$$F(h_s = A\cos\left[C\sin(h_s)\right] - B\sin\left[C\sin(h_s)\right] C = \frac{B_y}{\lambda}\cos(\delta)$$

We began by determining the known precessed declination of the source and assuming the wavelength $\lambda = 2.5cm$. To solve for the baseline B_y, we iterated over 500 values in the range of 700cm to 1200cm. For each value we saved the residuals, and chose the value corresponding to the minimum residual value as the optimal or ẗrue̗baseline length. We then used the coefficients from this regression to estimate τ_c, the cable delay.

2.4.3 Calculating diameter

We used similar signal processing techniques to filter the data for the Sun and the Moon. In the case of these data sets we attempted to preserve the envelope of the data, as it contains the information necessary to calculate radius.

We used a similar method of applying least squares as for the point source to fit an equation of the following form:

$$F(t) = \cos\left(2\pi\frac{B_y}{\lambda}\cos(\delta)sin(h_s) + \phi\right)$$

We chose not to use the baseline and cable delay calculated previously as they were very inconsistent. We attempted fitting both to the filtered data itself as well as its envelope calculated by convolving the absolute value of the data with a low pass filter. After obtaining this function by iterating over guesses of ϕ, just as solving when for B_y, we chose the corresponding value that minimized the error term.

The goal of doing all of this was to fit a function to the data over a narrow region to find the points at which it crossed 0. The envelope of the Sun and the Moon signals are ideally Bessel functions, which are functions of $R \cdot F_f$. By determining a fringe frequency F_f corresponding to the zero crossing, we matched that F_f to a value of F_f on the $R \cdot F_f$ axis of the Bessel function.

$$F_f = \left(\frac{B_y}{\lambda}\cos(\delta)\right)$$

To match the Bessel function with the envelope of the data, we used trial and error to shift it to a point which seemed to correspond to the measured data. Because the Bessel function crosses the x axis at integer values we can solve for the radius.

$$RF_f = \frac{k}{2}R = \frac{k}{F_f} = \frac{\lambda}{B_y\cos(\delta)\cos(h_s)}$$

We then multiplied this value of the radius in degrees by 2 to determine the angular diameters of the sources in degrees.

3 Results & Discussion

3.1 Point Source (3C144)

Figure 2 shows the raw data from observing 3C144 (the Crab Nebula) on 03/28/2014 beginning at 0:19:26 UTC. The power spectrum shows two peaks symmetric about zero that correspond to what we might expect to see as the output of the interferometer.

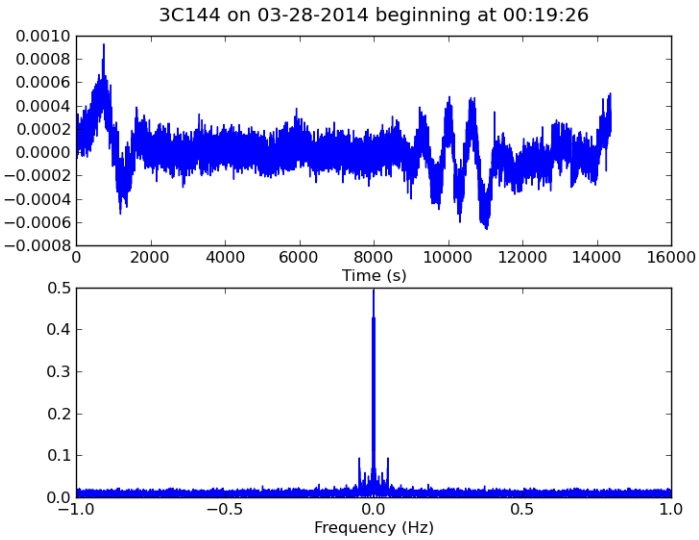

Figure 2: Raw data and power spectrum from the observation of 3C144 with the DC offset subtracted.

In order to isolate these peaks we first tested a variety of median filters. The result of applying median filters is shown in Figure 3. This low pass filtering eliminated many of the high frequency components due to repointing. We chose a window of size 9 so as not to eliminate frequencies surrounding the peak that may have been important.

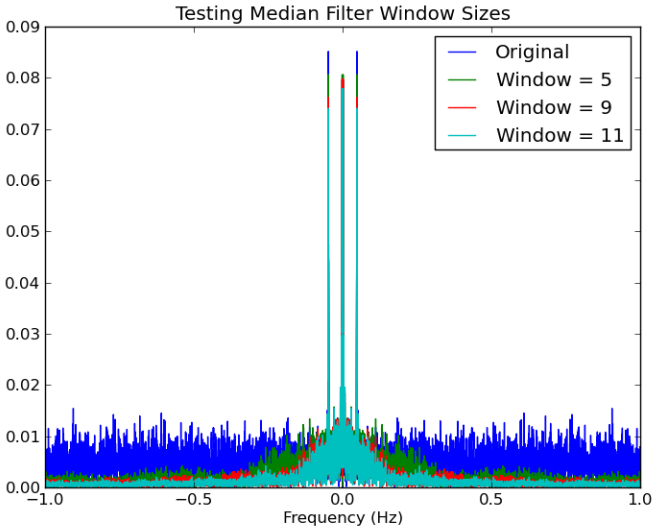

Figure 3: Effects of median filter with varying window sizes on the spectrum of the signal.

The data also appeared to have large irregularities in certain sections, of approximately 2000 seconds. This may have been due to other objects obstructing the telescope such as the other campus buildings mentioned previously. More likely however, these irregularities were probably caused by the repointing of the telescope as they occur both close to the beginning of the observation, as well as some point later in the observation. Interestingly the duration appears to be much longer than the time to run the homing procedure. In order to simplify the data processing we isolated a single segment of the raw data from 2000

to 6000 seconds (corresponding to the original observation. Figure 4 shows a plot of this data and that the amplitude of the assumed peaks of interest are much larger in the power spectrum.

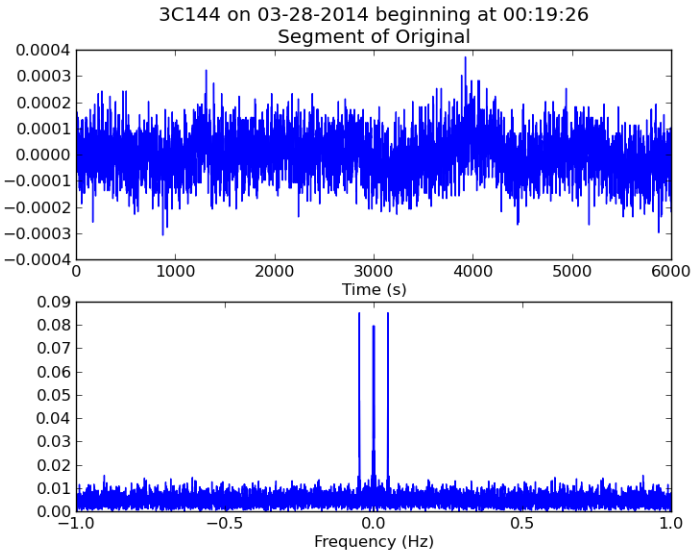

Figure 4: Segment of the raw data in which the frequency components of interest appear to be significantly stronger.

Continuing in the attempt to isolate the observed peaks, we next tested a series of FIR band pass filters to further isolate the peaks we noticed in the original spectrum. Figure 5 shows the result of applying these filters. Based on this we chose a filter with 256 taps centered around 0.05 Hz with a bandwidth of 0.01.

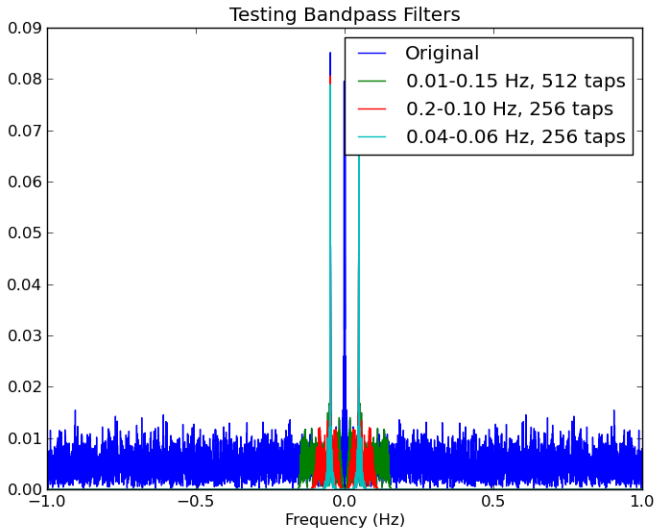

Figure 5: Effects of band pass filters with various parameters on the spectrum of the selected segment of the signal.

We also normalized the data to a range of -1 to 1 by dividing it by its maximum. The resulting filtered and normalized signal is shown in Figure 6.

After filtering the signal we applied least squares as described previously to fit a function to this data.

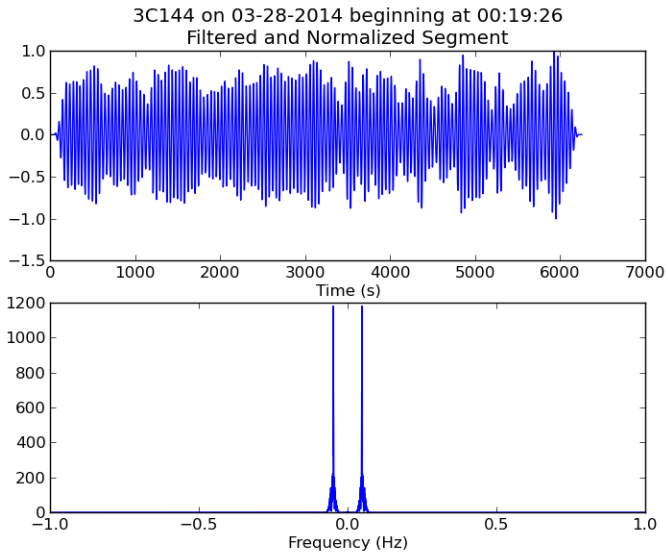

Figure 6: Result of filtering the selected segment of the signal to isolate the peaks visible in the unfiltered spectra.

Figure 7 shows the result. This simple attempt to use linear least squares appears to have some visual relationship to the data.

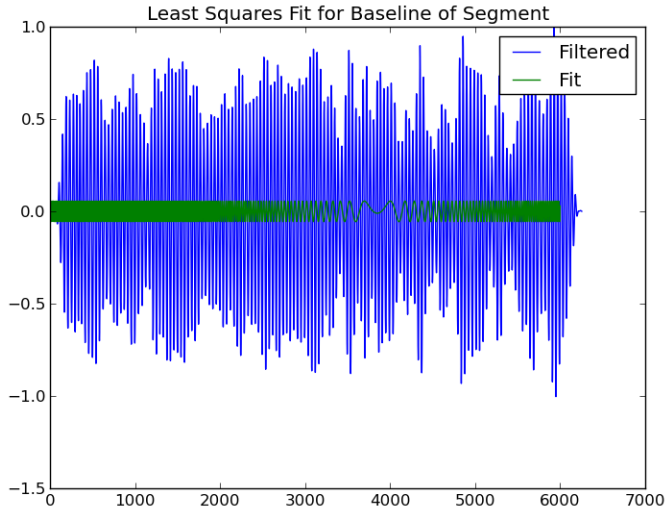

Figure 7: Result of least squares fitting to the filtered segment of the data.

Figure 8 shows the square of the residuals from applying least squares. The values are normalized to a maximum scale of 1. There is a noticeable minimum in this plot, however it corresponds to a value significantly lower than the known baseline of approximately 10m, and the scale of the difference between these values does not appear to be significant (less than 1%).

Considering the fringe frequency increases linearly with the baseline, we attempted to filter out other sections of the data to isolate a range that may include the actual fringe frequency. We chose values significantly higher than the peak visible in the original spectrum. The original observed peak produced

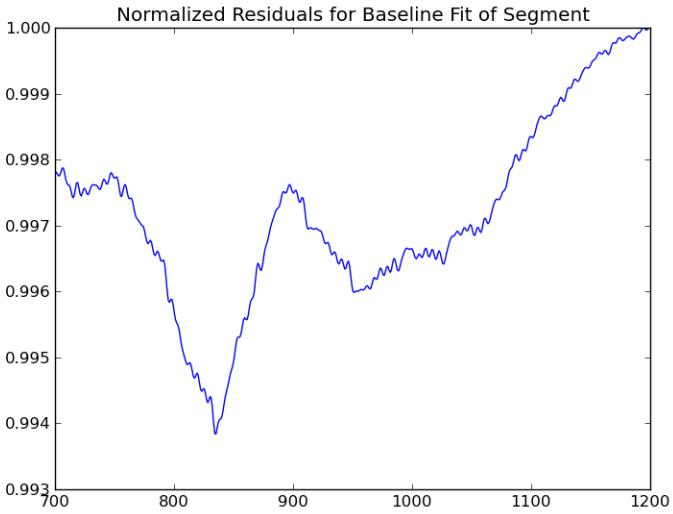

Figure 8: Residuals from fitting to the filtered segment of data. The residuals are plotted against the values of the baseline tested ranging from 700cm to 1200cm

a fairly obvious minimum error when applying least squares, so we chose a different part of the spectrum in the event that the visible peaks were not actually the fringe frequency of interest. The result of testing different band pass filters at higher frequencies is shown in Figure 9. We applied these filters to the original data set and ended up choosing an even narrower filter with a bandwidth of 0.005 Hz centered around 0.2 Hz.

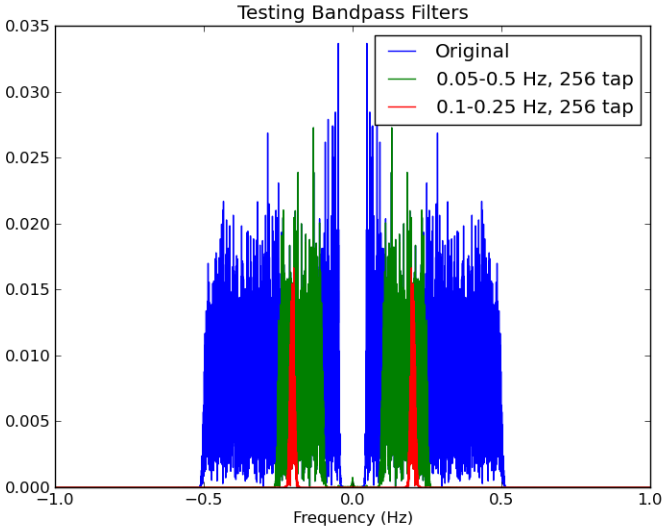

Figure 9: Effect of applying narrow band pass filters centered at higher frequencies.

The result of applying this filter is shown in Figure 10.

After filtering we attempted the same least squares analysis on this data. The result is shown in Figure 11.

Figure 12 shows the residual from applying least squares to this very narrow band of frequencies. Inter-

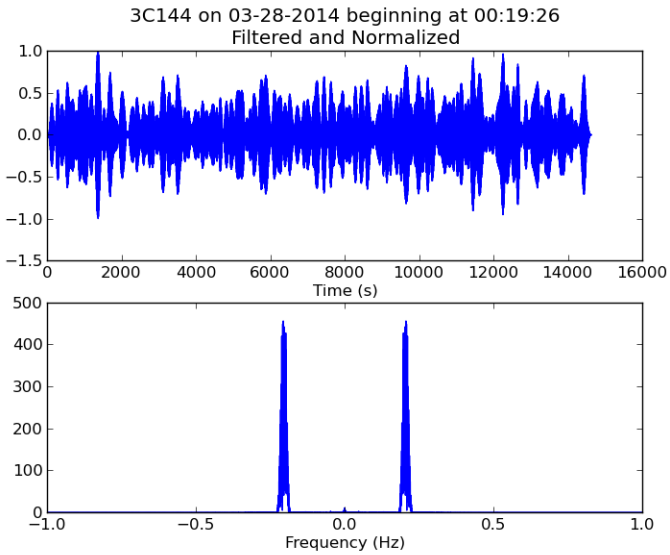

Figure 10: Result of applying a narrow band pass filter to isolate higher frequencies.

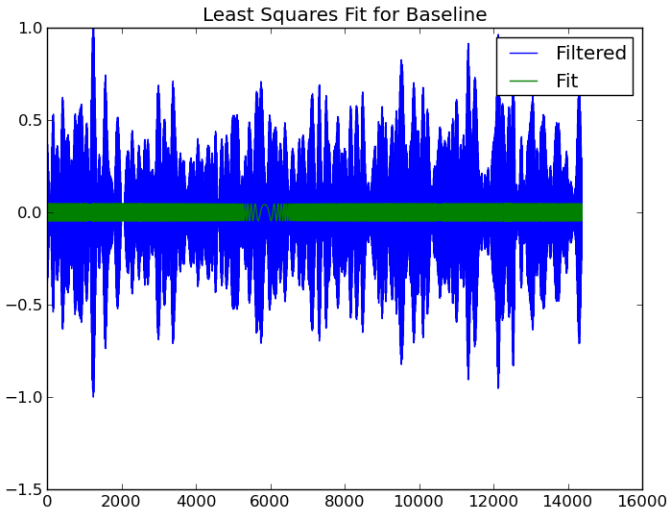

Figure 11: Result of applying least squares to fit a narrow band of higher frequencies.

estingly the resulting minimum error is more significant than the previous one (a difference of 6% between the most significant peaks compared to 0.2% with the previous analysis). The resulting value is also very close to the expected baseline of 10m, however the plot of the residuals still appears to vary significantly and has other local minima. This may simply be due to our attempt to apply this analysis technique intended for linear or affine functions to this problem. Although the hour angle does increase monotonically as explained in the lab document, $sin(h_s)$ can only be approximated by a linear function for a certain range.

While we were able to determine a value of the baseline $B_y = 1001.603cm$ close to the expected 10m, the fact that the range of frequencies we analyzed didn't correspond to the most noticeable peaks suggests the presence of some other strong source. We therefore applied the same least squares analysis to attempt to determine the of this source assuming a baseline length of 10m and varied $\cos(\delta)$ over a range of 0 to 90. We chose this range to eliminate the because we assumed the declination of the interfering source to be

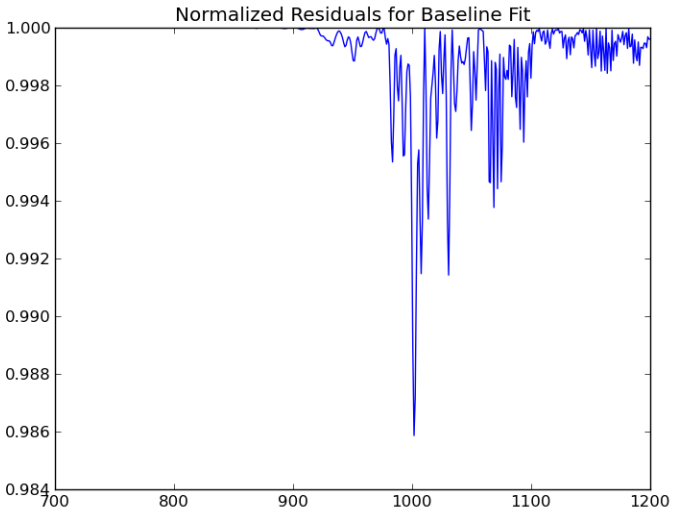

Figure 12: Residuals from applying least squares to fit a narrow band of higher frequencies. The residuals are plotted against the values of the baseline tested ranging from 700cm to 1200cm

similar to that of 3C144, and because analyzing the full range of $\cos(\delta)$ from -1 to 1 should produce roughly symmetric results. Figure 13 shows the result of this analysis.

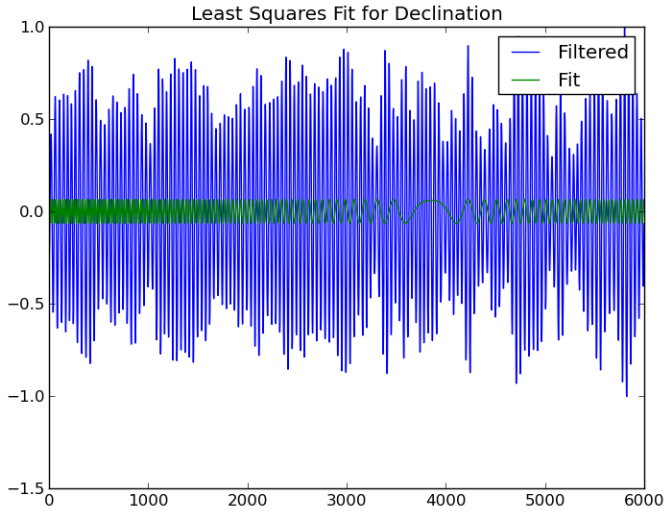

Figure 13: Result of applying least squares to fit a narrow band of higher frequencies.

When examining the residuals of this analysis in Figure 14, we can see that there are numerous local minima that do not differ significantly. Based on this analysis the determined value of δ was 64.620○. The lack of any noticeable peak above the noise in the spectrum close to these frequencies suggests that we were just analyzing noise as the interferometer correlates the outputs of the two telescopes.

Based on the coefficients from our least squares approximations we can also calculate the cable delay.

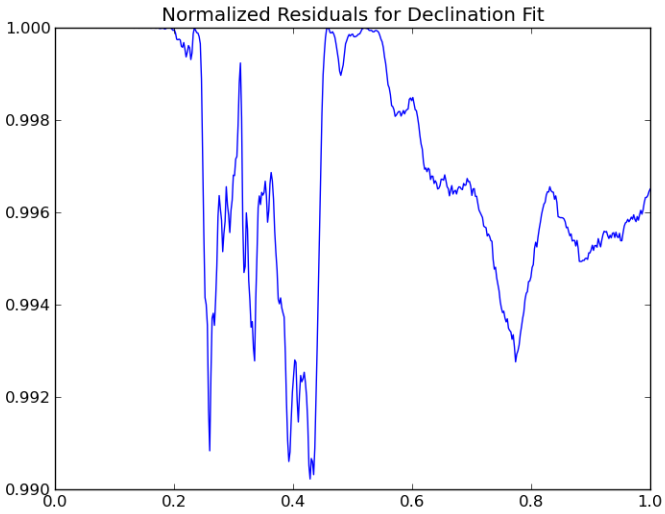

Figure 14: Residuals from applying least squares to fit a narrow band of higher frequencies. The residuals are plotted against the values of the $\cos(\delta)$ from 0 to 1.

First using the values from the fit to a narrow band of frequencies corresponding to roughly correct baseline:

$$\cos(2\pi\nu\tau_c) = A = -0.04549861\tau = \frac{\cos^- 1(A)}{2\pi\nu} = \frac{\cos^- 1(A)}{2\pi\frac{c}{\lambda}} = 2.1437 \times 10^{-11}$$

$$\sin(2\pi\nu\tau_c) = B = 0.00702375\tau = \frac{\sin^- 1(A)}{2\pi\nu} = \frac{\cos^- 1(A)}{2\pi\frac{c}{\lambda}} = 9.3159 \times 10^{-14}$$

Clearly the fact that this value is inconsistent shows that that our attempt to fit the data was imperfect. Using the coefficients from the attempt to fit declination yields even less promising results: $\tau_{cA} = 2.1682 \times 10^{-11}, \tau_{cB} = 4.1691 \times 10^{-11}$.

3.2 Sun

Figure 15 shows a plot of the raw data collected from a horizon to horizon observation of the sun on 4/2/2014 beginning at 15:31:05 UTC. Unlike the point source small ranges (over a few minutes) of the data were very obviously sinusoidal with roughly constant amplitude, however the overall shape of the data appears to be modulated by some function. Additionally due the peaks corresponding to these frequencies appeared to be much more obvious just from visually inspecting the spectrum.

The modulation of the sinusoid corresponds to the Fourier transform of the source intensity distribution. Assuming the sun is a 1D symmetric source, this corresponds to a Bessel function. Figure 16 shows a section of a Bessel function that appears to correspond to the measured data.

Overlaying the Bessel function and a segment of the sun data shows a fairly obvious relationship. While the plot in Figure 17 does not show the Bessel function as perfectly modeling the envelope of the measured sun data, it is roughly similar.

In order to calculate the radius, and therefore diameter of the sun, we applied the same least squares techniques to the data as previously explained. After obtaining the least squares approximation, we found the envelope of the function by applying a simple method for AM demodulation (low pass filtering the absolute value of the signal). The minimum of the envelope allowed us to more precisely determine the points at which the measured data crossed 0. Figure 18 shows the plots resulting from this analysis.

The residual shown in Figure 19 converges to a clear minimum unlike the previous analyses. The value of ϕ indicated by this plot appears to indicate a significant cable delay τ_c which is unlikely.

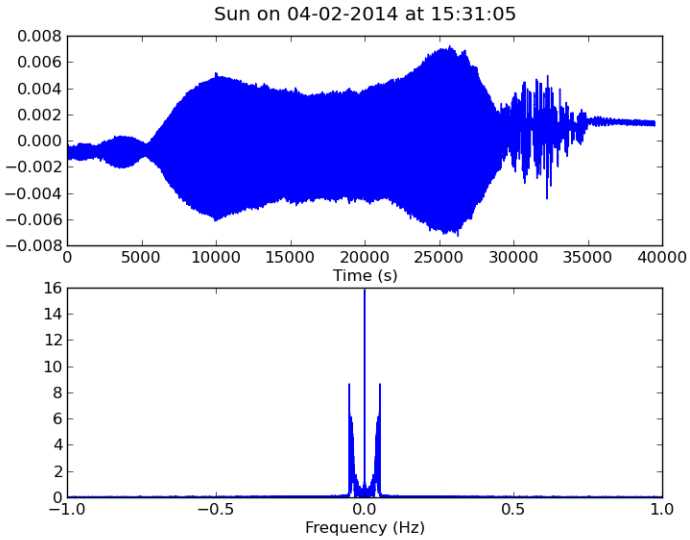

Figure 15: Raw data from the sun observation with the DC component subtracted such that the data is centered about 0.

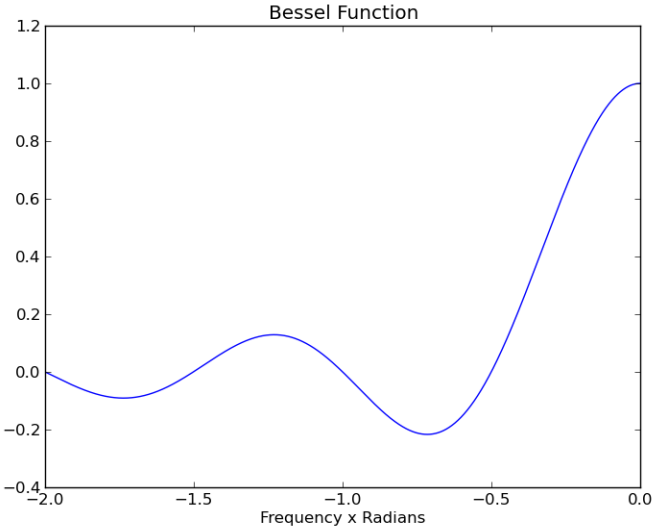

Figure 16: Ideal Bessel function

By using the hour angle h_s, declination δ, and known baseline and wavelength values corresponding to the time of the detected zero crossing, we were able to solve for the fringe frequency $F_f = \left(\frac{B_y}{\lambda}\cos(\delta)\right)$. As previously explained for the second zero crossing (which we know this value corresponds to from Figure 17, we calculated the angular radius after making the appropriate unit conversions to be $\frac{2}{2F_f} = 0.2156°$. The diameter is therefore 0.4312°.

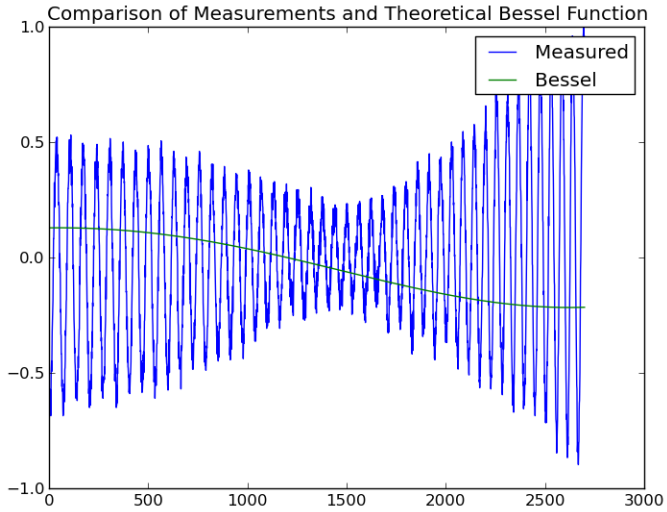

Figure 17: Comparison of a segment of sun data and ideal Bessel function.

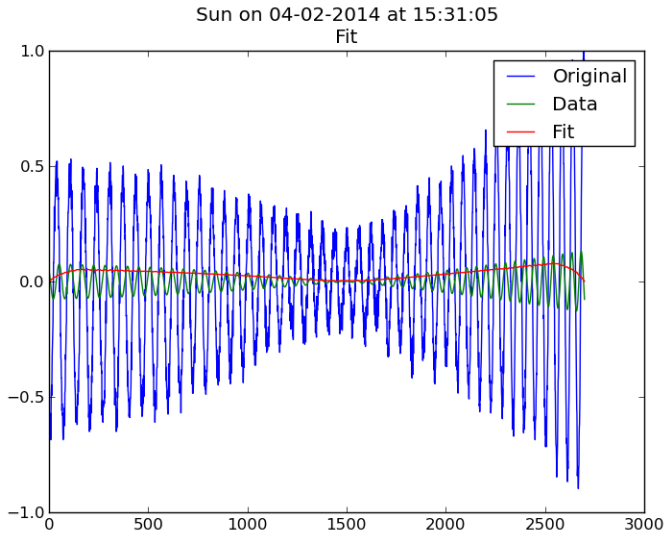

Figure 18: Least squares analysis to determine the local minimum of the sun data envelope.

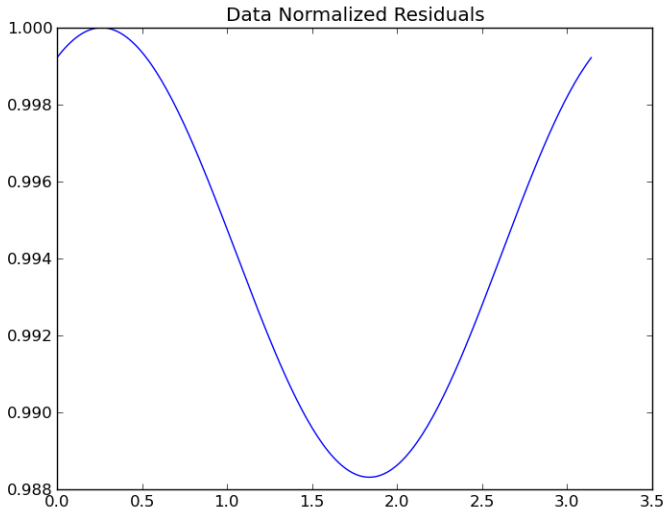

Figure 19: Residuals from least squares fitting.

3.3 Moon

We applied the same techniques used for the sun to the data from the moon. The raw data from our observation of the moon on 4/6/2014 beginning at 3:34:44 UTC is shown in Figure 20.

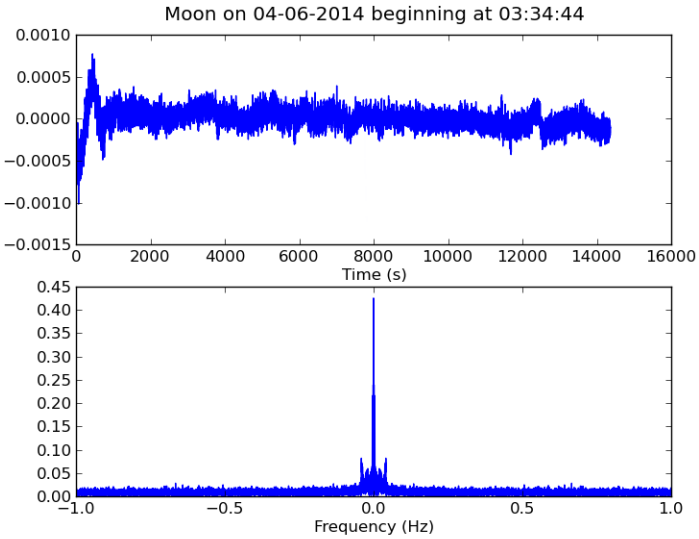

Figure 20: Raw data from the moon observation with the DC component subtracted such that the data is centered about 0.

The signal from the moon was significantly weaker considering the moon was only at approximately 30% of its maximum illumination at the point on the date of the observation and the shape of the envelope is much less obvious. The peaks corresponding to the fringe frequency are also visually smaller in the plot of the spectrum shown in Figure 20. We applied a band pass FIR filter with 256 coefficients centered about the observed peaks in the spectrum resulting in the plot shown in Figure 21. The filtered spectrum is also only a sub section of the data to remove the irregularities that occurred at roughly 1000 and 12000 seconds (likely due to the re-pointing of the telescope).

After filtering the signal does appear to have an envelope roughly corresponding to the shape of a Bessel function. Because we began observing the source shortly after it had passed the meridian on that day, we compared it to the right half of a Bessel function shown in 22.

As with the sun, we can identify the zero crossings corresponding to the Bessel function in our filtered data by overlaying the plots as shown in Figure 23.

We applied the same least squares techniques to determine the zero crossing of the filtered data 24. The residuals from this calculation are shown in Figure 25. The results of the residual are similar to the sun which intuitively makes sense considering we had similar data and used the procedure. As in the case of the sun, the minimum of the residuals seems to indicate that ϕ, corresponding to the cable delay τ_c which is still very significant unlikely.

We used the same equations to compute the radius of the moon to be $R = 0.17422°$. The diameter is therefore $D = 0.34844°$. This value is significantly smaller than the known diameter of the moon $D = 0.4922°$, however as shown the data was relatively noisy and our filtering may have affected frequencies of interest.

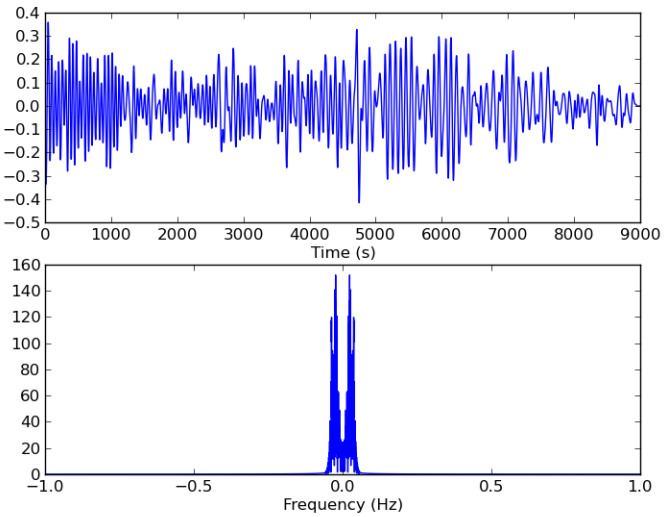

Figure 21: Result of applying a band pass filter to isolate the frequencies of interest in a segment of moon data.

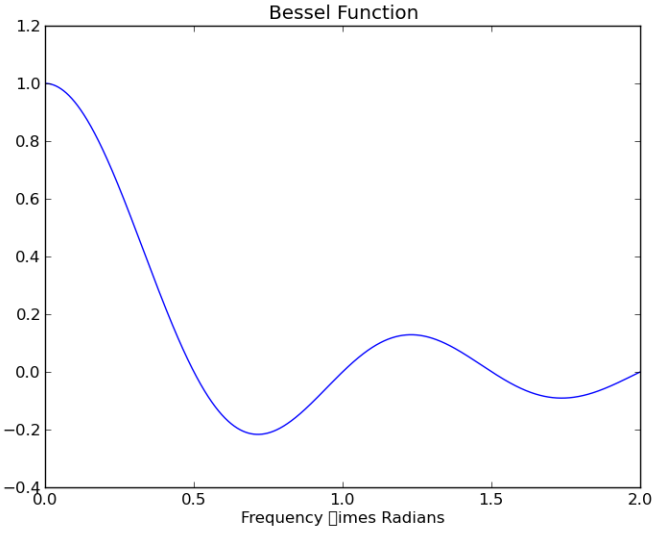

Figure 22: Ideal Bessel function

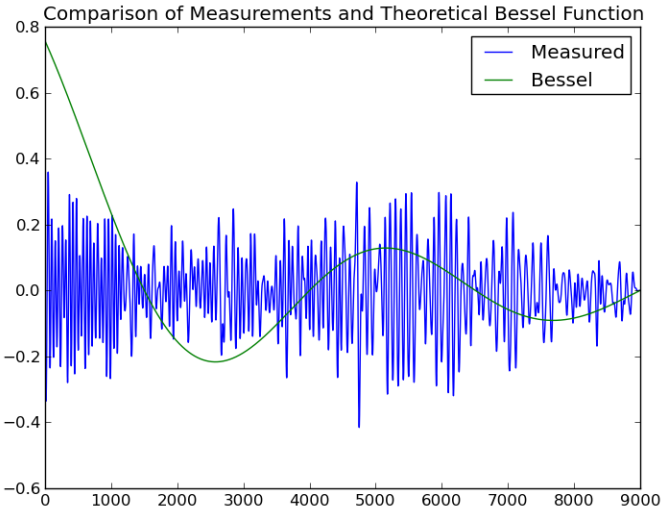

Figure 23: Comparison of a segment of filtered moon data and ideal Bessel function.

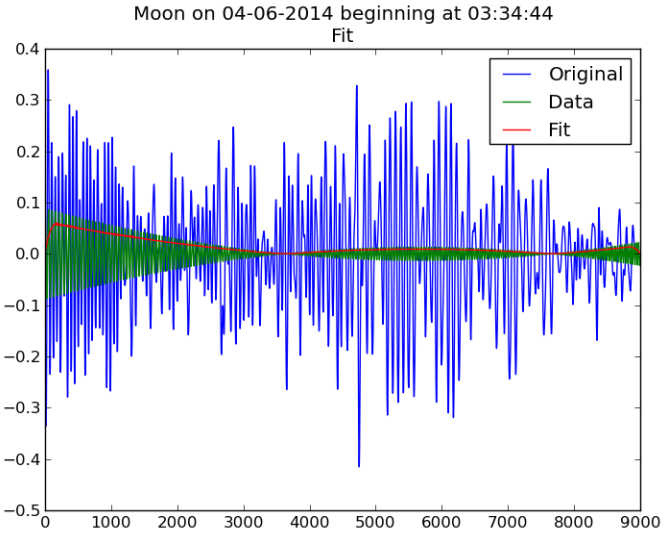

Figure 24: Least squares analysis to determine the local minimum of the moon data envelope.

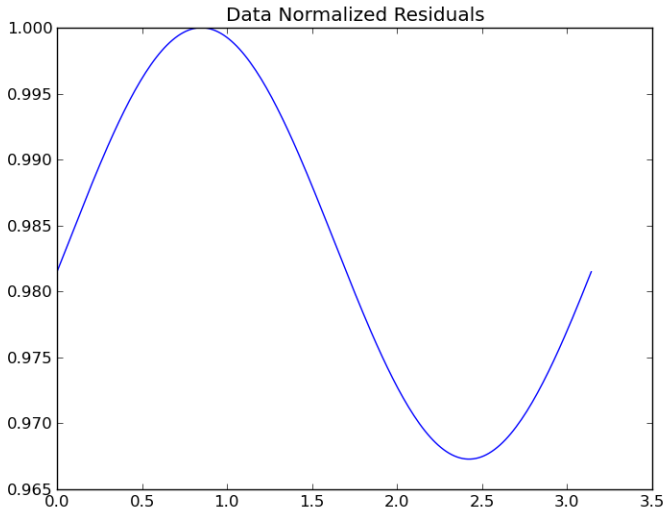

Figure 25: Residuals from least squares fitting.

4 Conclusion

This lab experiment was a valuable exercise in the applications of signal processing and data analysis. As expected, the data we recorded, despite the precautions we took to minimize error were far from ideal. We were able to compensate for this and achieve reasonable results by filtering out noise and using least squares to develop approximations of our data.

Code for the analysis and observation are not included in the body of this document but are both available online at: https://github.com/viyer/astro121. All original data and log files from the observations are available here as well.